Magnetic phase diagram of iron at high pressure and temperature

Agnès Dewaele*
CEA DAM-DIF, F-91297, Arpajon, France
and Université Paris-Saclay, CEA, Laboratoire Matière en Conditions Extrêmes, 91680 Bruyères-le-Châtel, France

Lucie Nataf
Synchrotron Soleil, F-91192 Saint Aubin, France

(Received 19 April 2022; accepted 28 June 2022; published 14 July 2022)

Crystallographic structure and long-range magnetic order of iron have been measured in pressure-temperature domains of 2–18 GPa and 300–800 K, using x-ray absorption spectroscopy and x-ray magnetic circular dichroism (XMCD) in resistively heated diamond anvil cells under hydrostatic pressurizing conditions. A fine coverage of pressure-temperature space allowed monitoring $\alpha \leftrightarrow \epsilon$, $\alpha \rightarrow \gamma$, and $\gamma \rightarrow \epsilon$ transformations, evidencing large metastability phenomena. α-Fe remains ferromagnetic under high pressure and temperature in its whole stability domain, and no magnetic response could be measured with XMCD in pure γ-Fe and ϵ-Fe. Structural and magnetic transformations are observed concomitantly within experimental uncertainties.

DOI: 10.1103/PhysRevB.106.014104

I. INTRODUCTION

Iron is perhaps the most famous example of allotropy in metals, in which magnetism, electron correlation, and lattice vibrations play an important role. Under ambient conditions, magnetism stabilizes the body-centered-cubic (bcc) α-Fe phase relative to close-packed structures adopted by metals of the same group, Os and Ru.

Under compression, α-Fe transforms into hexagonal close-packed (hcp) ϵ-Fe around 13 GPa at 300 K [1–4]. The $\alpha - \epsilon$ transformation has attracted a large interest for Fe-based materials technology as well as planetary science due to its prominent presence in terrestrial planet cores. It is considered as an archetypal pressure-induced martensitic transition with a mechanism following Burgers path [5,6]. There is evidence that ϵ-Fe is paramagnetic: the absence of any long-range magnetic order seen with Mossbauer spectroscopy and neutron diffraction, even under low temperature, [7–9], while x-ray resonance spectroscopy can see a magnetic signal in the stability domain of ϵ-Fe, up to ∼40 GPa, interpreted as a signature of a local magnetic moment on Fe atoms [9,10]. However, an antiferromagnetic order has been suggested in ϵ-Fe because it would lower the ground-state energy according to density functional theory modeling [11]. Some evidence of a magnetic ordering in the stability domain (close to the $\alpha - \epsilon$ transition) of ϵ-Fe has been collected [8,12], which suggests that structural and magnetic transformations are not coupled. In these studies, however, the structure was not measured at the same time as the magnetic response and is uncertain. As a matter of fact, the exact conditions of the $\alpha - \epsilon$ transition vary with experimental conditions such as sample microstructure or pressurizing conditions [4,5,10]. No measurement of the magnetic signature of the *reverse* $\epsilon \rightarrow \alpha$ transformation has been performed, although its mechanism differs from the direct one [5].

Heated at ambient pressure, α-Fe loses ferromagnetic ordering at Curie temperature $T_C = 1043$ K and transforms into a fcc γ-Fe phase at 1188 K. Early measurements in large volume devices showed that Curie temperature does not depend on pressure, suggesting that above a Curie-γ-α triple point around 1.8 GPa and 1040 K, the $\alpha - \gamma$ transition is also a ferromagnetic to paramagnetic one [13,14]. However, to our knowledge, no magnetic characterization of the $\alpha - \gamma$ transition has been performed above 2 GPa. $\alpha - \gamma$ and $\alpha - \epsilon$ equilibrium lines intersect to form an $\alpha - \gamma - \epsilon$ triple point [14]. The estimations of the location of this point are surprisingly scattered, with pressure varying between 7.9 and 10.5 GPa and temperature between 678 and 753 K (see Ref. [15] for a review).

X-ray magnetic circular dichroism (XMCD) is a useful technique to investigate the magnetic properties of 3d transition metals in diamond anvil cells; it does not require a particular sample environment, is element and orbital selective, and is sensitive to small magnetic moments [16]. XMCD compares the x-ray absorption spectra of one sample immersed under two magnetic fields with opposite directions. It it thus sensitive to a magnetic moment averaged over space (on the volume scanned with x rays) and collection time. Under ambient conditions, α-Fe produces a clear XMCD signal at the Fe K edge [17], which is interpreted by a modification of the 4p band, directly scanned with x-ray absorption, induced by the 3d magnetic moment. On pressure increase, the XMCD signal disappears, but different studies report a collapse preceding [10,17] or accompanying [18] the structural α-Fe $\rightarrow$ ϵ-Fe transition at 300 K. The Monza *et al.* study [10] is particularly interesting as the magnetic and structural transitions have been decoupled by the use of

*agnes.dewaele@cea.fr

a particular sample nanostructure; in this sample, the early loss of ordered magnetism suggests that it could be a driving force for the structural $\alpha \rightarrow \epsilon$ transformation. Among the above-mentioned studies, only one has been carried out using quasihydrostatic pressurizing conditions [18]. To our knowledge, XMCD has not been employed to characterize the magnetism of iron in the high-temperature regime; high-temperature magnetic measurements are scarce above 0.5 GPa and have been performed on a limited number of (P, T) points [13,19].

Here, we establish a high-pressure–high-temperature structural and magnetic phase diagram of iron, based on x-ray absorption spectroscopy (XAS—to measure the crystalline structure) + XMCD diagnostics, in the 2–18 GPa and 300–800 K domain. This domain includes the $\alpha - \gamma - \epsilon$ triple point. Experiments are conducted in diamond anvil cells, under hydrostatic pressurizing conditions, and direct and reverse transformations are monitored. Measurements under high temperature also present technical advantages: a temperature increase reduces the α-ϵ pressure coexistence domains [15], allowing a tighter constraint on the phase transformation conditions; it allows providing purely hydrostatic pressurizing conditions in rare-gas solids pressure media, such as neon, above its melting curve [20]. We try to provide answers to the following questions: Can a temperature increase allow decoupling of the magnetic and structural $\alpha \leftrightarrow \epsilon$ transitions, such as a microstructure in Ref. [10]? Is the structural transition driven by magnetism loss or the opposite? What is the sequence of structural and magnetic transformations for the reverse $\epsilon \rightarrow \alpha$ transformation? Does α-Fe keep ferromagnetic order on temperature increase up to the $\alpha \rightarrow \gamma$ structural transformation, contrary to the situation at ambient pressure?

II. EXPERIMENTAL METHODS

Samples, i.e., cylinders of 120 μm diameter and 5 μm thickness, have been cut with an fs laser in an iron foil (Goodfellow, 99.99% purity). They were loaded in diamond anvil cells (DACs) equipped with 400 μm culet single-crystal diamonds, with standard or Almax-Boehler design. To reduce x-ray absorption by the anvils, the total diamond thickness was kept below 2.9 mm by the use of one perforated diamond. SrB_4O_7:Sm^{2+} was placed in the high-pressure chamber for pressure measurement purposes; the calibration of Ref. [21] has been used, modified with the recent update [22]. The pressure transmitting medium was neon, except in one run for which Daphne 7474 oil was used [23]. Gaskets were made of rhenium.

The DACs were made with an Cu-Be (at 300 K) or an amagnetic inconel alloy which allows heating up to at least 800 K; they were placed in a resistive heater in an enclosure which temperature was continuously monitored. The temperature on the sample was measured a few times in each run to establish the sample vs oven temperature relationship.

The oven has been inserted into the magnetic area of the ODE beam line at synchrotron SOLEIL [16], for x-ray absorption spectroscopy (XAS) and XMCD measurements under a magnetic field of 0.9 T (1.2 T for one ambient-temperature run). The measurement geometry was conventional, with the magnetic field parallel to the diamond anvil cell compression axis and x-ray beam. The x-ray spot size was $\sim 30 \times 30$ μm FWHM and typical exposure times for samples in the DAC were 100×300 ms for each XAS spectrum collected in the 7.06–7.33 keV energy range, repeated for 5 to 15 $\pm\vec{B}$ cycles for the collection of one XMCD spectrum, which lasted at least 30 minutes.

XAS and XMCD spectra have been recorded under various pressure-temperature conditions spanning from 1.5 to 18 GPa, 300 to 790 K, mostly following isotherms with 0.5 to 1 GPa pressure steps. The orientation of the cell was optimized at the beginning of each run to minimize the parasitic signal in the XAS spectra due to diffraction by diamond anvils. The pressure was measured on-line before and after each XMCD spectrum collection, with a difference of less than 0.2 GPa on average, yielding a total uncertainty on pressure of 0.3 GPa. Above 720 K, the luminescence signal of SrB_4O_7:Sm^{2+} was too weak to allow pressure measurement and the pressure was estimated from sample pressure vs membrane pressure systematics, with an estimated uncertainty of ± 1 GPa. In most cases, the pressure transmitting medium was a liquid which ensured purely hydrostatic pressurizing conditions of the sample. Low-pressure 300 K XAS and XMCD signals were recorded at the end of each run to check the absence of any irreversible change such as a chemical reaction of the sample. In all cases, α-Fe with an XMCD signal close to the starting one was recovered below 7 GPa and 300 K.

III. MEASUREMENTS

A. XAS and macroscopic magnetism in pure α-Fe, ϵ-Fe, and γ-Fe

Figure 1 shows typical XAS spectra recorded in three different samples under varying conditions. A comparison with the literature data shows that they are typical of bcc, hcp, and fcc crystallographic phases of iron [17,18,24]. This corresponds to the α-Fe, ϵ-Fe, and γ-Fe phases, respectively. The XAS spectra of the fcc and hcp phases are close, as the local structure around the atoms is almost the same in these two close-packed phases; however, they can be distinguished by the features indicated by arrows around 7.13 keV [24]. The XAS spectrum of the bcc phase clearly differs from the hcp and fcc phases, in particular with features around 7.137 keV (indicated by an arrow in Fig. 1), 7.205 keV, and 7.220 keV, as discussed in Mathon *et al.* [17]. We have processed the XAS spectra with ATHENA software [25]. $\chi(k)k^2$, which is calculated by normalizing and subtracting the background of the XAS spectrum, and its Fourier transform exhibit similar oscillations and frequencies to Ref. [18] for α-Fe and ϵ-Fe (see Fig. 2). However, due to the limited k range of the current measurements, the Fourier spectrum plotted on the right part of Fig. 2 is imprecise and does not allow extraction of information such as lattice parameters.

XAS data recorded in this study have thus been quantitatively interpreted to identify the sample phase following Mathon *et al.*'s method, which is more suited for XAS spectra collected in a limited energy range. The energy derivatives of XAS at two energies (7.137 and 7.205 keV) have been calculated. Here their sum is called the XAS derivative

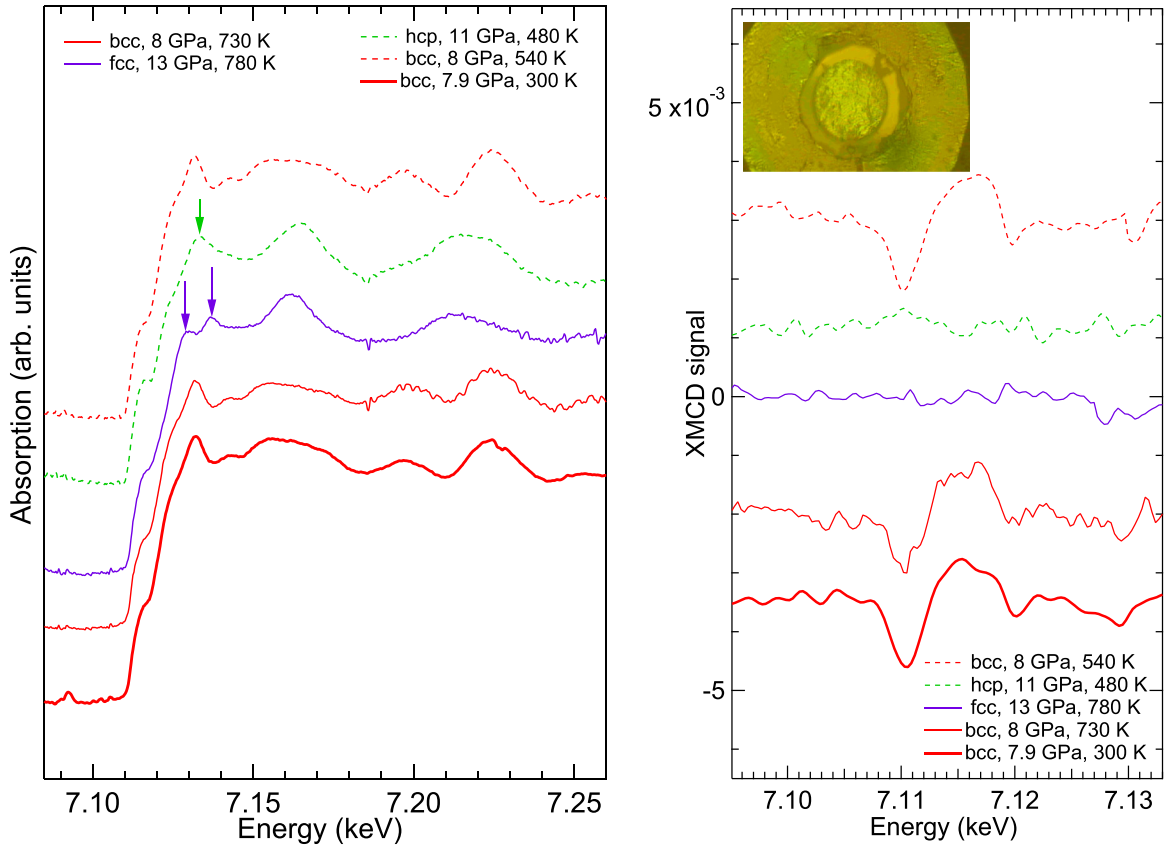

FIG. 1. Left: X-ray absorption spectra measured in three iron samples under varying P/T conditions. The inset shows the energy derivative of absorption; it is different in the bcc, fcc, and hcp phases around 7.137 keV. Right: XMCD signal recorded around 7.115 keV. Macroscopic magnetization can be measured in α-Fe (red curves), and no signal is recorded in ϵ-Fe and γ-Fe. The inset is a photograph of the high-pressure cavity for one run (sample diameter 130 μm).

signal and is used to distinguish α-Fe from ϵ-Fe or γ-Fe. It is shown in Fig. 3 for one pressure ramp, together with raw XAS spectra.

Figure 4 presents pressure/temperature (P/T) conditions where pure α-Fe, ϵ-Fe, or γ-Fe have been identified; they agree very well with a published iron phase diagram [15], taking into account the hysteresis of the phase transformations. In pure phases, the changes in the XAS spectra are weak in the scanned pressure/temperature range: Figure 1 shows that temperature increase between 300 and 730 K has no measurable effect on the XAS signal of α-Fe; a pressure increase shifts the XAS features toward higher energies due to the reduction of interatomic distances [24].

Figure 1 shows the XMCD signal collected at the same time as XAS at the Fe K edge in pure phases. In α-Fe, a signal similar to that in Refs. [17,18] is recorded between 7.10 and 7.13 keV. The XMCD amplitude is measured by a fit of the data points by the same function as the ambient conditions XMCD (plotted in Fig. 3), after subtraction of a continuous background signal. It has been theoretically shown that the XMCD signal is due to the interaction of the excited 4p photoelectrons with the spin-polarized 3d bands of the neighboring

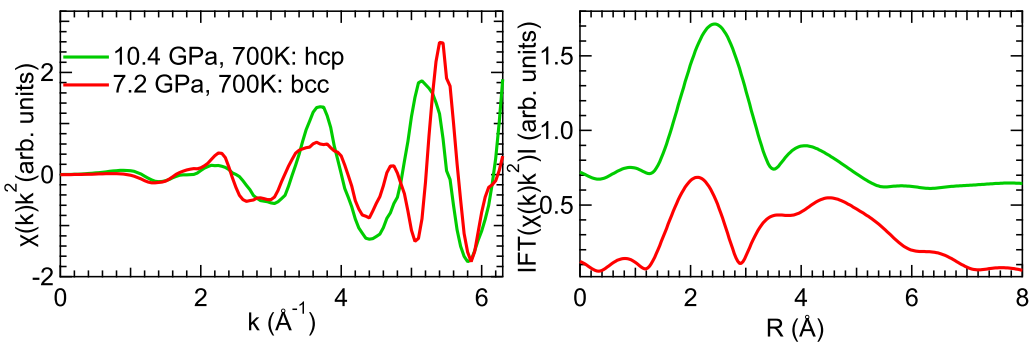

FIG. 2. Left: $\chi(k)k^2$ profiles obtained from typical XAS spectra recorded in α-Fe, ϵ-Fe, and γ-Fe. Right: Magnitude of the Fourier transform of $\chi(k)k^2$. The curves have been shifted from each other for clarity.

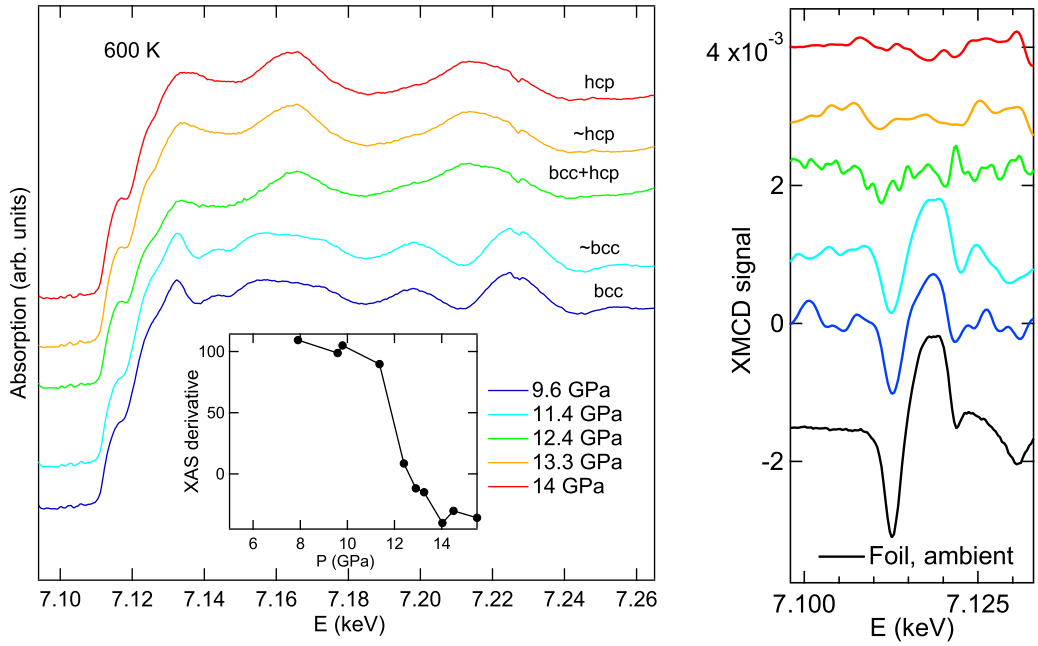

FIG. 3. Left: Evolution of XAS spectra recorded on pressure increase along a 600 K isotherm. Inset: Corresponding XAS derivative signal as a function of pressure, which allows estimation of the amount of α-Fe (bcc) and ϵ-Fe (hcp) in the sample. Right: Corresponding XMCD spectra. The reference spectrum collected with an iron foil under ambient conditions and used for the measurement of the XMCD amplitude is plotted as a black line.

atoms [26]. We then assume, as in earlier works, that its amplitude is proportional to the average magnetic moment of the 3d

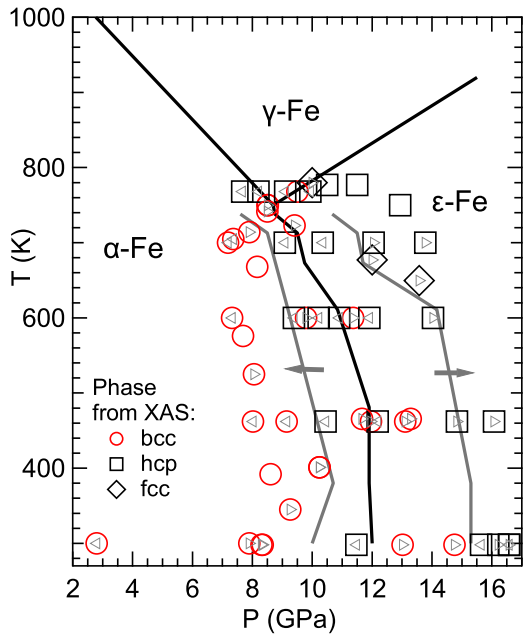

FIG. 4. Pressure-temperature conditions where the XAS signal of a *pure* bcc, hcp, or fcc signal has been recorded, compared with $\alpha \leftrightarrow \epsilon$ transformation lines (continuous gray lines) and equilibrium lines estimated in Ref. [15] (continuous black lines). Triangles indicate if the data have been collected on pressure increase ($\triangleright$) or decrease ($\triangleleft$). ϵ-Fe/α-Fe are metastable on pressure decrease/increase and γ-Fe is metastable on temperature decrease, which explains why the phases are observed out of their stability field.

bands in the sample [17,18]. Here, the amplitude of the signal measured under magnetic field of 0.9 T (high-temperature runs) is 75% of the amplitude of the signal measured under a magnetic field of 1.2 T (ambient-temperature runs), which suggests that samples are not fully saturated under 0.9 T. This is likely due to the shape anisotropy factor in the DAC sample, which strongly diminishes the efficiency of a magnetic field to magnetize a flat sample with its surface perpendicular to the field [27]. This could affect XMCD measurements if the shape anisotropy factor was varying in the course of the experiment; that is not the case here, as the iron foil is compressed in a hydrostatic pressure transmitting medium and no other deformation than a small elastic strain ($\leqslant$3.5% according to the Fe equation of state [15]) is expected. To confirm this, we checked that the XMCD signals measured in α-Fe at the beginning and the end of each run were identical.

In α-Fe, the amplitude of the XMCD signal slightly decreases with increasing temperature, but remains at least 80% of its maximum value up to a α-Fe $\rightarrow$ γ-Fe transformation (see Fig. 1); it is not affected by a pressure increase. The weak effect of temperature on magnetization measured around 8 GPa, compared to ambient-pressure measurements [28], suggests that the Curie temperature in α-Fe does not vary with pressure in its whole stability range, confirming the trend measured up to 2 GPa [13,14]. In pure ϵ-Fe and γ-Fe, no magnetic signal is recorded (within experimental uncertainty due to measurement noise, which represents $\sim$10% of maximum XMCD signal), which suggests that these phases do not have any ferromagnetic order (an antiferromagnetic order is possible).

In the next section, we present and discuss measurements collected in $P-T$ domains where phases of iron coexist.

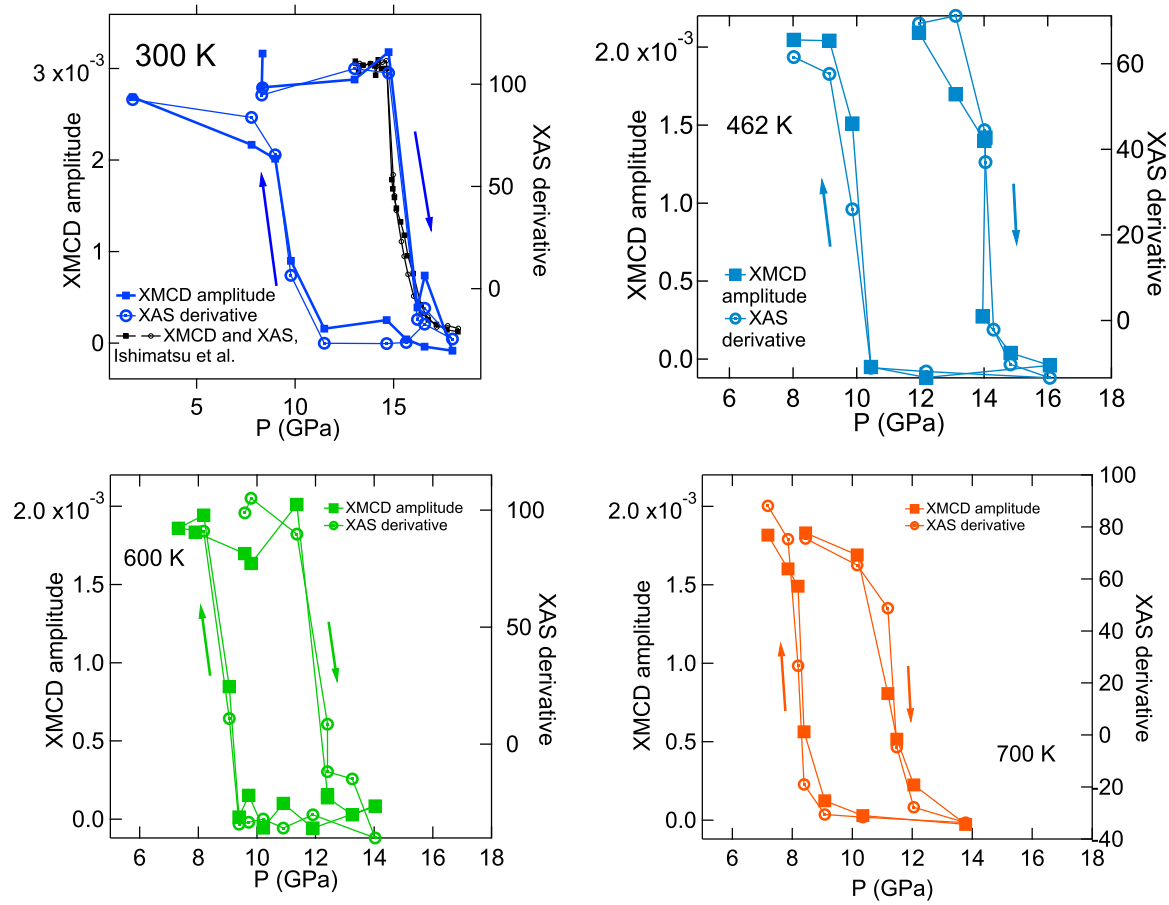

FIG. 5. Iron XMCD signal amplitude and XAS derivative signal (defined in text) as a function of pressure along pressure cycles at four different temperatures below the $\alpha - \epsilon - \gamma$ triple point. The measurements have been made in three runs (same run for 600 K and 700 K isotherms). The magnetic field was 1.2 T at 300 K and 0.9 T at high temperature. The 300 K graph also presents Ref. [18] measurements (XMCD amplitude and bcc/hcp phases fraction, scaled to the present data) made under hydrostatic conditions.

B. XAS and macroscopic magnetism in mixed phases

1. α-ϵ transformation

Figure 5 presents values of the XMCD amplitude and XAS derivative signal measured during α-Fe $\rightarrow$ ϵ-Fe $\rightarrow$ α-Fe cycles along four isotherms. These signals are constant within $\pm 2.5 \times 10^{-4}$ and ± 10, for the XMCD and XAS derivative, respectively, in extended pressure domains (pure phases domains, see the above discussion) and abruptly vary in 1.2 to 2.5 GPa pressure intervals, which we interpret as mixed phase domains. The volumetric amount of each phase can be directly estimated from the XAS signal derivative, with a $\sim$10 vol.%. accuracy (estimated from the data scatter).

The hysteresis in the transformation reported previously [3–5,15] is obvious; it decreases with increasing temperature, as observed in Ref. [15]. The conditions of direct and reverse transformations are summarized in Table I and are in excellent agreement with the recent literature [15].

Figure 5 shows that the XMCD amplitude varies in parallel with XAS, from a maximum value in α-Fe to a negligible value in ϵ-Fe. XAS and XMCD data recorded at 300 K during the direct α-Fe $\rightarrow$ ϵ-Fe transformation agree very well with

TABLE I. Temperature T (in K) and pressure P (in GPa) conditions of α-Fe $\rightarrow$ ϵ-Fe ($\uparrow$) and ϵ-Fe $\rightarrow$ α-Fe ($\downarrow$) transformations. "50% phase" corresponds to an equal volumetric amount of α-Fe and ϵ-Fe; "50% XMCD" indicates a value of XMCD amplitude corresponding to 50% of its maximum value. ΔP indicates the approximate width of the phases' coexistence domains (in GPa).

T (K)	$P_{50\%\ \text{phase}}\uparrow$	$\Delta P_{\text{phase}}\uparrow$	$P_{50\%\ \text{XMCD}}\uparrow$	$\Delta P_{\text{XMCD}}\uparrow$	$P_{50\%\ \text{phase}}\downarrow$	$\Delta P_{\text{phase}}\downarrow$	$P_{50\%\ \text{XMCD}}\downarrow$	$\Delta P_{\text{XMCD}}\downarrow$
300	15.5	2.0	15.5	2.5	9.4	2.4	9.4	2.4
462	14.2	1.6	14.2	1.8	9.8	1.3	10	1.3
510					9.1	0.8	9.3	1.2
600	12.4	2.0	12.4	1.0	8.8	1.2	9.0	1.2
700	11.3	2.0	11.2	1.5	8.3	1.5	8.3	1.5

TABLE II. Conditions of temperature and pressure of XAS and XMCD measurements in two runs [see Fig. 6, with XAS derivative signal and XMCD amplitude, in the order they have been taken (first 12 lines: first run)]. Typical values of the XAS derivative signal are $\sim 85 \pm 10$, -5 ± 10, and -70 ± 10 for α-Fe, ϵ-Fe, and γ-Fe, respectively. When XMCD amplitude is not provided, this means that no XMCD signal could be detected. No meas. indicates that no measurement has been performed.

T (K)	P (GPa)	XAS derivative signal	Phase	XMCD amplitude	T (K)	P (GPa)	XAS derivative signal	Phase	XMCD amplitude
392	8.61	95.05	α	0.00171	462	12.2	−3.3	ϵ	
576	7.68	83.15	α	0.00190	462	10.4	−2.0	ϵ	
668	8.16	80.02	α	0.00176	462	9.9	48.5	$\epsilon+\alpha$	0.00139
714	7.90	78.09	α	0.00170	462	9.1	91.0	α	0.00182
741	8.5	66.84	α	0.00151	462	8.0	96.4	α	0.00191
780	9	70.08	$\alpha+\gamma$	0.00141	525	8.1	89.9	α	0.00191
780	10	−19.55	$\alpha+\gamma$	0.00023	723	9.4	81.1	α	0.00198
677	12	−65.46	γ		750	8.5	78.6	α	0.00224
649	13.57	−72.86	γ	0.00016	750	8.5	80.5	α	no meas.
484	13.47	−64.32	γ		768	9.5	79.2	α	0.00211
300	12.18	−55.47	$\gamma+\epsilon$	0.00017	777	10.5	1.7	$\alpha+\epsilon$	
300	2.8	90.60	α	0.00191	777	11.5	0.8	ϵ	
462	11.9	106.0	α	0.00196	750	12.9	4.7	ϵ	
462	13.1	108.9	α	0.00193	768	9.9	4.3	ϵ	
462	14.0	71.8	$\alpha+\epsilon$	0.00084	768	9.1	1.4	ϵ	
462	14.0	61.9	$\alpha+\epsilon$	0.00110	768	8.2	2.5	ϵ	
462	13.9	9.7	$\alpha+\epsilon$	0.00017	768	7.7	5.7	ϵ	
462	14.8	−1.0	ϵ		705	7.6	76.4	$\alpha+\epsilon$	0.00183
462	16.1	−5.2	ϵ		705	7.4	79.3	α	no meas.
					345	9.3	96.9	α	0.00185

the Ishimatsu *et al.* data [18], represented in black in Fig. 5. Experimental conditions were similar in the two studies (hydrostatic pressurizing conditions, foil sample). The conditions of magnetic transitions, summarized in Table I, are almost the same as the conditions of the structural $\alpha \leftrightarrow \epsilon$ transitions, within ± 0.2 GPa. This difference is within uncertainties of pressure measurement (accuracy of measurements and small pressure drift during data collection). This coincidence is a strong hint that in the scanned pressure-temperature range, ϵ-Fe has no ferromagnetic order and bcc α-Fe keeps its ferromagnetic order up to structural transformation.

2. α-γ transformation

$\alpha \rightarrow \gamma$ transformation has been monitored in one run following the pressure-temperature path presented in Fig. 4. γ-Fe is synthesized at 770 K around 8 GPa, a temperature above the $\alpha - \gamma - \epsilon$ triple point (8.7 GPa and 750 K), which evidences a hysteresis for the $\alpha - \gamma$ transition, as measured earlier [6,15]. γ-Fe is largely metastable on temperature decrease in the stability field of ϵ-Fe, a behavior that has been reported by other authors [15,29]; here, this effect is striking as a mixture of γ-Fe and ϵ-Fe is observed down to 300 K at 12 GPa. Both phases disappear on pressure decrease and the sample reverts to pure α-Fe at 2.8 GPa and 300 K.

The $\alpha \rightarrow \gamma$ structural transformation evidenced with XAS coincides with the magnetic one, with an XMCD signal which vanishes when α-Fe disappears (see Table II). It is below the detection limit and remains so in γ-Fe and ϵ-γ mixtures. The full XMCD signal is recovered in α-Fe.

We tried to induce a $\epsilon \rightarrow \gamma \rightarrow \alpha$ transformation by pressure decrease around 8 GPa and 768 K. Instead, a direct $\epsilon \rightarrow \alpha$ transition was observed (see Fig. 6) with a concomitant reemergence of the XMCD signal, evidencing metastability phenomena under conditions close to the triple point. This

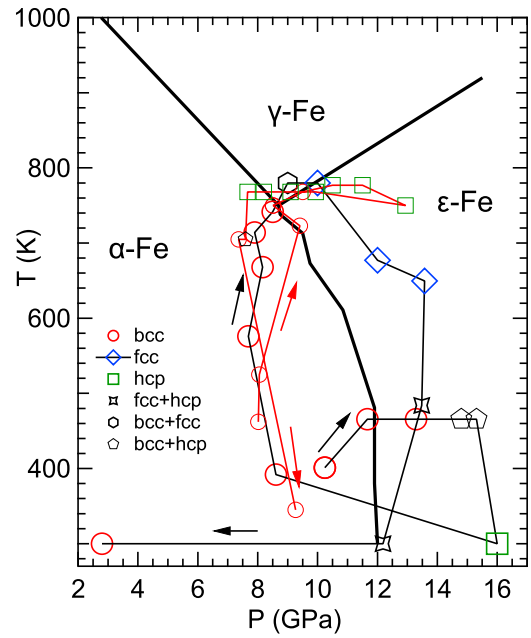

FIG. 6. Parts of pressure-temperature paths followed in the two highest-temperature runs carried out in this study. The symbols indicate which phase or phases' mixture has been identified with XAS.

explains why the location of the α-Fe, γ-Fe, and ϵ triple point is so difficult to measure.

IV. DISCUSSION

In this work, no loss of ferromagnetism is observed by temperature increase in pure α-Fe under high pressure, up to 740 K at 8.5 GPa (e.g., very close to the conditions of $\alpha \rightarrow \gamma$ transformation). The magnetic moment measured with XMCD disappears at the same time as the structural $\alpha \rightarrow \gamma$ transformation. This is different from the situation at ambient pressure, where the magnetic transformation precedes the structural one by 140 K [14]. The $\alpha \rightarrow \gamma$ transformation mechanism, which has been demonstrated to involve soft phonon modes in paramagnetic phases at ambient pressure [30,31], might thus differ under high pressure. A theoretical modeling of a bcc-fcc structural and magnetic transformations in Fe is needed.

We confirm the absence of macroscopic magnetization measured with XMCD in pure bulk ϵ-Fe at 300 K, as obtained previously [10,17,18]. In addition, we find that ϵ-Fe exhibits no magnetization under high temperature up to the triple point, 750 K [15]. The loss/recovery of the magnetic moment coincides with the $\alpha \rightarrow \epsilon/\epsilon \rightarrow \alpha$ structural transition, within 0.2 GPa, between 300 and 700 K. Such an accuracy could be obtained by hydrostatic pressurizing conditions which reduce the phases' coexistence domains to less than 2 GPa and allows a tight constraint on the phase transformation conditions. On the other hand, the abruptness of the transitions does not allow one to test an interesting hypothesis such as an enhanced magnetic susceptibility of α-Fe in mixed phases [8], which would create a high XMCD signal in samples containing low amounts of α-Fe.

The current observation is in line with Mossbauer and neutron diffraction measurements, which were unable to detect any signature of a magnetic ordering in ϵ-Fe [7–9]. The recent technique of nitrogen-vacancy centers has been used to measure the magnetization of iron grains loaded in a diamond anvil cell vs pressure. It has been found that at 300 K, magnetization of the grains disappears at the same time as the α-Fe phase, even if this can be at a pressure that is higher than expected, around 20 GPa [12,32]. This is likely due to the nonhydrostatic pressure medium used in these studies (nitrogen, argon, or NH_3BH_3), which increases the $\alpha - \epsilon$ coexistence domain [4]. Similarly, magnetic remanence values typical of ferromagnets measured up to 18 GPa in Ref. [8] can be attributed to α-Fe, which can be kept up to that pressure under nonhydrostatic compression [4], maybe with an increased susceptibility. X-ray emission spectroscopy studies measure that the local magnetic moment on Fe atoms is below detection limits above ~30–40 GPa [9,10]. One recent theoretical study predicts the existence of short-lived local magnetic moments in paramagnetic ϵ-Fe [33] at 30 GPa, linked to superconducting behavior. XMCD is not able to detect such magnetic phenomena.

To sum up, here we show that the phase diagram long-range magnetic order in iron measured under high hydrostatic pressure and temperature closely mimics its structural phase diagram: α-Fe remains ferromagnetic in its whole structural stability domain; the $\alpha \leftrightarrow \epsilon$, $\alpha \leftrightarrow \gamma$, and magnetic transitions are sharp; and no evidence of a magnetic order is found in γ-Fe and ϵ-Fe. We suggest that the persistence of a ferromagnetic response in the ϵ-Fe stability domain reported earlier is attributed to untransformed α-Fe, which is retained under nonhydrostatic compression. The fine coverage of the phase diagram performed here evidences metastability/hysteresis phenomena for all transitions in Fe, particularly important for γ-ϵ transformations. Pressure increase does not favor magnetism, and thus we do not expect any reemergence of a magnetic signal above 30 GPa, where the local magnetic moment on Fe atoms is observed to vanish.

ACKNOWLEDGMENTS

We acknowledge SOLEIL for provision of synchrotron radiation facilities under Proposals No. 20180409, No. 20191556, and No. 20201400. We thank Florent Occelli for the diamond anvil cells designs and help with samples loadings, and Jean Coquet and Anojh Thevarasan for their assistance during data acquisition.

[1] D. Bancroft, E. L. Peterson, and S. Minshall, Polymorphism of iron at high pressure, J. Appl. Phys. **27**, 291 (1956).

[2] T. Takahashi and W. A. Bassett, High-pressure polymorph of iron, Science **145**, 483 (1964).

[3] P. M. Giles, M. H. Longenbach, and A. R. Marder, High pressure alpha-epsilon martensitic transformation in iron, J. Appl. Phys. **42**, 4290 (1971).

[4] R. Boehler, N. V. Bargen, and A. Chopelas, Melting, thermal expansion, and phase transitions of iron at high pressure, J. Geophys. Res. **95**, 21731 (1990).

[5] A. Dewaele, C. Denoual, S. Anzellini, F. Occelli, M. Mezouar, P. Cordier, S. Merkel, M. Véron, and E. Rausch, Mechanism of the alpha-epsilon transformation in iron, Phys. Rev. B **91**, 174105 (2015).

[6] E. Boulard, C. Denoual, A. Dewaele, A. King, Y. Le Godec, and N. Guignot, Following the phase transitions of iron in 3D with x-ray tomography and diffraction under extreme conditions, Acta Mater. **192**, 30 (2020).

[7] D. L. Williamson, S. Bukshpan, and R. Ingalls, Search for magnetic ordering in hcp iron, Phys. Rev. B **6**, 4194 (1972).

[8] Q. Wei, C. McCammon, and S. A. Gilder, High-pressure phase transition of iron: A combined magnetic remanence and Mössbauer study, Geochem. Geophys. Geosys. **18**, 4646 (2017).

[9] B. W. Lebert, T. Gorni, M. Casula, S. Klotz, F. Baudelet, J. M. Ablett, T. C. Hansen, A. Juhin, A. Polian, P. Munsch, G. Le Marchand, Z. Zhang, J.-P. Rueff, and M. d'Astuto, Epsilon iron as a spin-smectic state, Proc. Natl. Acad. Sci. USA **116**, 20280 (2019).

[10] A. Monza, A. Meffre, F. Baudelet, J.-P. Rueff, M. d'Astuto, P. Munsch, S. Huotari, S. Lachaize, B. Chaudret, and A. Shukla, Iron Under Pressure: "Kohn Tweezers" and Remnant Magnetism, Phys. Rev. Lett. **106**, 247201 (2011).

[11] G. Steinle-Neumann, L. Stixrude, and R. E. Cohen, First-principles elastic constants for the hcp transition metals Fe, Co, and Re at high pressure, Phys. Rev. B **60**, 791 (1999).

[12] M. Lesik, T. Plisson, L. Toraille, J. Renaud, F. Occelli, M. Schmidt, O. Salord, A. Delobbe, T. Debuisschert, L. Rondin, P. Loubeyre, and J.-F. Roch, Magnetic measurements on micrometer-sized samples under high pressure using designed NV centers, Science **366**, 1359 (2019).

[13] V. D. Blank and E. I. Erskin, *Phase Transitions in Solids under High Pressure* (CRC Press, Boca Raton, FL, 2014).

[14] L. J. Swartzendruber, The fe system, Bull. Alloy Phase Diagr. **3**, 161 (1982).

[15] A. Dewaele, V. Svitlyk, F. Bottin, J. Bouchet, and J. Jacobs, Iron under conditions close to the alpha-gamma-epsilon triple point, Appl. Phys. Lett. **112**, 201906 (2018).

[16] F. Baudelet, Q. Kong, L. Nataf, J. D. Cafun, A. Congeduti, A. Monza, S. Chagnot, and J. P. Itié, Ode: A new beam line for high-pressure XAS and XMCD studies at SOLEIL, High Press. Res. **31**, 136 (2011).

[17] O. Mathon, F. Baudelet, J. P. Itié, A. Polian, M. d'Astuto, J. C. Chervin, and S. Pascarelli, Dynamics of the Magnetic and Structural $\alpha-\varepsilon$ Phase Transition in Iron, Phys. Rev. Lett. **93**, 255503 (2004).

[18] N. Ishimatsu, Y. Sata, H. Maruyama, T. Watanuki, N. Kawamura, M. Mizumaki, T. Irifune, and H. Sumiya, $\alpha-\epsilon$ transition pathway of iron under quasihydrostatic pressure conditions, Phys. Rev. B **90**, 014422 (2014).

[19] J.-P. Rueff, M. Mezouar, and M. Acet, Short-range magnetic collapse of Fe under high pressure at high temperatures observed using x-ray emission spectroscopy, Phys. Rev. B **78**, 100405(R) (2008).

[20] W. L. Vos, J. A. Shouten, D. Young, and M. Ross, The melting curve of neon at high pressure, J. Chem. Phys. **94**, 3835 (1991).

[21] F. Datchi, R. LeToullec, and P. Loubeyre, Improved calibration of the SrB_4O_7:Sm^{2+} optical pressure gauge: Advantages at very high pressures and high temperatures, J. Appl. Phys. **81**, 3333 (1997).

[22] G. Shen, Y. Wang, A. Dewaele, C. Wu, D. E. Fratanduono, J. Eggert, S. Klotz, K. F. Dziubek, P. Loubeyre, O. V. Fat'yanov, P. D. Asimow, T. Mashimo, R. M. M. Wentzcovitch, and other members of the IPPS task group, Toward an international practical pressure scale: A proposal for an ipps ruby gauge (ipps-ruby2020), High Press. Res. **40**, 299 (2020).

[23] K. Murata, K. Yokogawa, H. Yoshino, S. Klotz, P. Munsch, A. Irizawa, M. Nishiyama, K. Iizuka, T. Nanba, T. Okada, Y. Shiraga, and S. Aoyama, Pressure transmitting medium daphne 7474 solidifying at 3.7 GPa at room temperature, Rev. Sci. Instrum. **79**, 085101 (2008).

[24] R. Torchio, A. Monza, F. Baudelet, S. Pascarelli, O. Mathon, E. Pugh, D. Antonangeli, and J. P. Itié, Pressure-induced collapse of ferromagnetism in cobalt up to 120 GPa as seen via x-ray magnetic circular dichroism, Phys. Rev. B **84**, 060403(R) (2011).

[25] B. Ravel and M. Newville, ATHENA, ARTEMIS, HEPHAESTUS: Data analysis for x-ray absorption spectroscopy using IFEFFIT, J. Synchrotron Rad. **12**, 537 (2005).

[26] O. Šipr and H. Ebert, Theoretical fe $L_{2,3}$- and k-edge x-ray magnetic circular dichroism spectra of free iron clusters, Phys. Rev. B **72**, 134406 (2005).

[27] H. Kronmuller and M. Fahnle, *Micromagnetism and the Microstructure of Ferromagnetic Solids* (Cambridge University Press, Cambridge, 2003).

[28] J. Crangle and G. M. Goodman, The magnetization of pure iron and nickel, Proc. R. Soc. London A **321**, 477 (1971).

[29] T. Komabayashi, Y. Fei, Y. Meng, and V. Prakapenka, *In situ* x-ray diffraction measurements of the γ-ϵ transition boundary of iron in an internally heated diamond anvil cell, Earth Planet. Sci. Lett. **282**, 252 (2009).

[30] J. Neuhaus, M. Leitner, K. Nicolaus, W. Petry, B. Hennion, and A. Hiess, Role of vibrational entropy in the stabilization of the high-temperature phases of iron, Phys. Rev. B **89**, 184302 (2014).

[31] I. Leonov, A. I. Poteryaev, Y. N. Gornostyrev, A. I. Lichtenstein, M. I. Katsnelson, V. I. Anisimov, and D. Vollhardt, Electronic correlations determine the phase stability of iron up to the melting temperature, Sci. Rep. **4**, 5585 (2015).

[32] L. Toraille, A. Hilberer, T. Plisson, M. Lesik, M. Chipaux, B. Vindolet, C. Pépin, F. Occelli, M. Schmidt, T. Debuisschert, N. Guignot, J.-P. Itié, P. Loubeyre, and J.-F. Roch, Combined synchrotron x-ray diffraction and NV diamond magnetic microscopy measurements at high pressure, New J. Phys. **22**, 103063 (2020).

[33] A. S. Belozerov, A. A. Katanin, V. Y. Irkhin, and V. I. Anisimov, Magnetic fluctuations and superconducting pairing in epsilon-iron, Phys. Rev. B **101**, 155126 (2020).